RESEARCH ARTICLE

The effect of $MgCl_2.6H_2O$ and NaF on properties of Chitosan / HA-Al_2O_3 Scaffold

Fatemeh Mirjalili [1*], Ali Kafashiyan [2], Esmail Salahi [3]

[1] Department of Material Engineering, Maybod Branch, Islamic Azad University, Maybod, Iran

[2] Department of Material Engineering, Yazd Branch, Islamic Azad University, Yazd, Iran

[3] Energy and Environmental Department, Materials and Energy Research Center, Karaj, Iran

ARTICLE INFO

Article History:
Received 2021-01-20
Accepted 2021-04-18
Published 2021-05-01

Keywords:
Nano
Scaffold
HA
Alumina
Chitosan/ HA- Al_2O_3 scaffold

ABSTRACT

The HA- Al_2O_3 nano composite was produced by precipitation method. In the first study,
the effect of MgCl2.6H2O and NaF additives on HA-Al_2O_3 nano-composite powder were studied and the second, chitosan / HA- Al_2O_3 scaffold was prepared by freeze casting method. The phase and microstructure and morphology analysis of nano composite and scaffold were performed by XRD, FT-IR, FESEM and TEM. X-ray diffraction test results along with infrared spectroscopy indicated that, the HA- Al_2O_3 nano composite without impurities were produced. TEM result showed that, the produced nano cmposite particle sizes were reported between 30-50 nm.
Moreover, the porosity percentages of scaffold without additive was about 56% and with NaF as an additive was about 63 %, however, the scaffold with $MgCl_2.6H_2O$ additive with 70% porosity had the highest porosity percentage. The compressive strength of the SFA scaffold exhibited a two-fold strength compared to the SMA scaffold, which indicated the improved mechanical compatibility of the SFA scaffold.

How to cite this article
Mirjalili F., Kafashiyan A., Salahi E. The effect of $MgCl_2.6H_2O$ and NaF on properties of Chitosan / HA-Al_2O_3 Scaffold . J. Nanoanalysis., 2021; 8(2): 135-144. DOI: 10.22034/jna.005.

INTRODUCTION

Bone regeneration is a complex cascade of biological events which controlled by numerous molecules and provides signals at local injury sites allowing progenitors and inflammatory cells to migrate and trigger healing processes. Conventional tissue engineering strategies utilize combination of cells, biodegradable scaffolds and systemic administration of bioactive molecules to promote natural processes of tissue regeneration and development [1-3]. A number of strategies for controlled biomolecule delivery from scaffolds have been developed for bone tissue engineering. One of the most common methods to achieve controlled and localized release of biomolecules is to incorporate them within biomaterials during the phase of scaffold fabrication [4]. According to this approach, the properties of the scaffolds, such as pore size and crosslinking density can control the biomolecule release rate by diffusion. In addition, the rate of scaffold degradation affects the biomolecule release rate over a prolonged time period [5-6]. Implantation of bone auto grafts or allografts is a simple strategy to heal large bone defects [7]. However, there are some drawbacks of these strategies which limit their widespread usage, such as extended surgical time and donor site morbidity for auto graft and adverse immune response and pathogen disease transmission for allograft. These problems have guided researchers for the development of bone substitute materials [8–12]. As the most promising bone substitute materials, calcium phosphate (CP) compounds have been widely used clinically due to their similarity to hard tissues [13].

* Corresponding Author Email: *Fm.mirjalili@gmail.com*

Among different CP ceramics hydroxyapatite (HA) and tri-calcium phosphate (TCP), or combinations of these two materials (biphasic ceramics) have gained special attentions for a wide range of applications such as maxillofacial reconstruction [14-16], orbital implants [17], spine fusion [18] and repair of bone defects [19]. These materials have been clinically used in dense, granular and porous forms [20–22]. Hydroxyapatite is calcium phosphate nearest to bone mineral and the most thermodynamically stable phase in the body [2, 23]. Calcium phosphates, such as hydroxyapatite for their biocompatibility and similarity to the mineral components of bones and teeth are good replacements for parts of the body which are damaged [1, 24]. Hydroxyapatite increases the capability of bone growth and forms a strong chemical bond with bone tissue when the bone tissue grow in the surface layer of this ceramic [3,25]. Nonetheless it is a brittle material which leads to low mechanical failure and limits its application in a position under the load. Therefore, it is important to add a secondary phase to improve the strength and mechanical properties of hydroxyapatite. The most important materials such as alumina, zirconia, titania and organic glass can be used as the reinforcing components [4, 26]. Due to its unique thermal, mechanical, and chemical properties, alumina is applied widely in the strong materials, composites and reinforcing materials. Alumina as the engineering ceramic based on its high mechanical properties and biocompatible properties is used as bone and dental fittings [5, 27]. Moreover, its application in biology increases owing to hardness, high strength against fatigue and resistance to corrosion [28]. NaF and $MgCl_2$.$6H_2O$ nanocrystalline ceramics have biocompatibility and bioactivity and similarities to bone mineral parts in many bone marrow engineering scaffolds, metal surface coatings, and drug delivery and delivery [29].

The replacement of various ions such as sodium (Na), magnesium (Mg), fluorine (F), chlorine (Cl), aluminum (Al) improves chemical composition and structure of apatite. Ion substitution in the apatite structure not only leads to improving the biocompatibility, bioactivity, mechanical properties which are similar to the apatite body in terms of chemical composition, but also it decreases the therapy course and bone repair significantly[30-32]. To date, various methods such as electrically [11, 32], freeze drying [33], solvent casting [22], fusion separation, and other methods for the construction of scaffolding for application in tissue engineering by researchers has been studied. In 2009, a study was conducted on the effect of fluoride additive on the mechanical properties of hydroxyapatite/alumina composites for increasing the strength of the scaffold [18, 20, 34]. Researchers have been studying the effects of MgF_2 on animal skin and have not reported any toxicity [19]. Synthesized hydroxyapatite nanoparticles was done by adding of NaF and carbonate. Hydro-deformed apatite had increased the formation of the diameter of the apatite layer between the scaffold and the bone [13, 20]. In 2017, a study was conducted on the mechanical and cytotoxic properties of 3d printed multi-compartment capsular devices. The results confirmed that, the scaffold containing 15% of hydroxyapatite had more mechanical and biocompatible properties [35]. The researchers conducted a study on the construction of a hydroxyapatite-gelatin scaffold for bone reconstruction on rat rats. It was observed that, the use of this scaffold increased the speed of repair of bone tissue [35]. Moreover, the researchers constructed a composite scaffold of chitosan / polyvinyl alcohol / carbon nanotubes by electrostatic method. Polyvinyl alcohol was used as a surfactant to stabilize carbon nanotubes [36].

This study has driven us to verify and prepare nanocomposite of HA- Al_2O_3 with different additives and then, the chitosan/ HA- Al_2O_3 scaffold was systematized. The novelties of this research are investigating the effects of NaF and $MgCl_2.6H_2O$ on preparing the nanocomposite of HA- Al_2O_3 as well as on the morphology and the microstructure properties of produced nanocomposite. Also, preparing the scaffold of chitosan / HA- Al_2O_3 as well as the microstructure, mechanical, cell viability and compatibilities of produced scaffold were investigated.

EXPERIMENTALS

Preparation of Hydroxyapatite-Alumina nano composite powder

Hydroxyapatite-alumina nano composite powder was prepared by precipitation method.

At first, suspension of 0.4 M $Ca(NO_3)_2\,4H_2O$ (Merck, prolabo 0308821 142) and $(NH_4)_2HPO_4$ (Merck, prolabo A0143307 037) was prepared. Then, 0.239 M $(NH_4)_2\,HPO_4$ solution was added drop wise to $Ca(NO_3)_2\,4H_2O$ solution and stirred for 2 h and added to first solution (solution 1).

Next, $MgCl_2.6H_2O$ and NaF additives with weight percent of 10 wt% were added to solution 1[30]. In the next step, aluminum nitrate (LobaChemie 7784-27-2) was prepared in distilled water and mixed for 1 h (solution 2) and aged for 24 h. Then, the second solution was added to the first solution. The final solution was mixed for 2 h and aged for 24 h. After filtering and washing, the materials were dried and calcined at 1200 °C for 1 h.

Preparation of chitosan/ HA- Al_2O_3 scaffold

In order to build the scaffolding, the freeze casting method was used. At first, 2 gr chitosan was dissolved in100 ml of acetic acid solution of 1 % at 75 °C for 30 minutes and then 0.4 gr gelatin was added and homogenized at 100 °C for 12 h. Then, 25% of hydroxyapatite /alumina with two different additives powder made in the previous steps was added to the hydrogel and homogenized for 48 h at 120 ° C. After that, the sample was transferred to a 24-house dish and placed at an initial temperature of -20 °C for 24 h for initial freezing. Then, the scaffold was prepared in two freeze-dried steps. In the first stage, it was placed in the freezer dryer for 24 h at a temperature of -80 °C and placed in the glutamate solution of 25% for 24 h after leaving the scaffold. Then, after two washing steps with ethanol of 96% and hot water, the scaffold was again placed inside the freezer for 24 h. X-ray diffraction (XRD, PW1800, Philips) was used for phase identification.

A crystalline size of powders was determined by the Scherrer method as follow:

$$t = 0.89\,\lambda / \beta \cos\theta \qquad (1)$$

Therefore, t is grain size, the wave length is λ and β is peak width and the angle in degrees is θ [30]. Field emission scanning electron microscope (FESEM) and transition electron microscopy (TEM, PHENOM) were conducted for investigation of microstructures and morphology of powders. Test samples were loaded at a testing machine (Instron 5569, Instron corp., Canton, U.S.) to measure the compressive strengths at a crosshead speed of 1 mm/min.

The apparent density and porosity of nano composite was measured using the Archimedes method. In the next step, the proliferation and survival of L929 cells on the surface of the samples were evaluated by MTT (3-(4,5-Dimethylthiazol-2-Yl)-2,5-Diphenyltetrazolium Bromide) assay. To prepare the samples, a common protocol for this test was used. In this way, 5 mg of each of the samples was mixed in the medium and incubated at 37 ° C for 72 h. These samples were filtered to prevent contamination. After extracting the cells desired in the culture plate, number of wells was considered as controls and some were considered as the test samples. After the desired time, the culture medium was discarded and a certain volume of solution was spilled on the cells and then, the cells were incubated in this solution. At this time, the MTT ring was broken, breaking the ring created crystalline purplish color. The amount of this color was directly related to the living cells. Next, the supernatant was discarded and the cells were washed. At the end, the absorbance of the solution was calculated by the spectrophotometer.

The following formula is then used to determine the survival rate:

$$\text{Cell Viability\%} = \frac{ODs}{ODc} \qquad (2)$$

ODs Optical Density Sample, ODc Optical Density Control [2].

Cell culture and cell membrane propagation were used on scaffolds from the rats' tail (929L) cells. In the next step, the proliferation and survival of L929 cells on the surface of the samples were evaluated by MTT assay [5, 31]. Statistical comparison of data from t-student method was performed. All experiments were assayed in triplicate.

RESULTS AND DISCUSSIONS:

Synthesis of Hydroxyapatite Alumina nano composite powder with different additives

The XRD pattern of the HA- Al_2O_3nano composite powders with and without additives was shown in Fig 1. The XRD pattern in Fig 1 indicated that, the samples was mostly HA and another crystalline phase of Tricalcium phosphate phase (T) existed (Sample H) . By adding of 10% $MgCl_2.6H_2O$, the Magnesium phosphate (M) was formed (Sample J) and with addition of 10% NaF, the formation of Sodium fluorophosphates (N) was achieved (Sample M).

The crystalline sizes and crystalline degrees of HA-Al_2O_3 nano composite powders with and without additives were explained at Table 1.

As Table 1 indicated, by increasing the $MgCl_2.6H_2O$, the crystalline sizes were reduced and crystalline degrees of nanocomposites increased

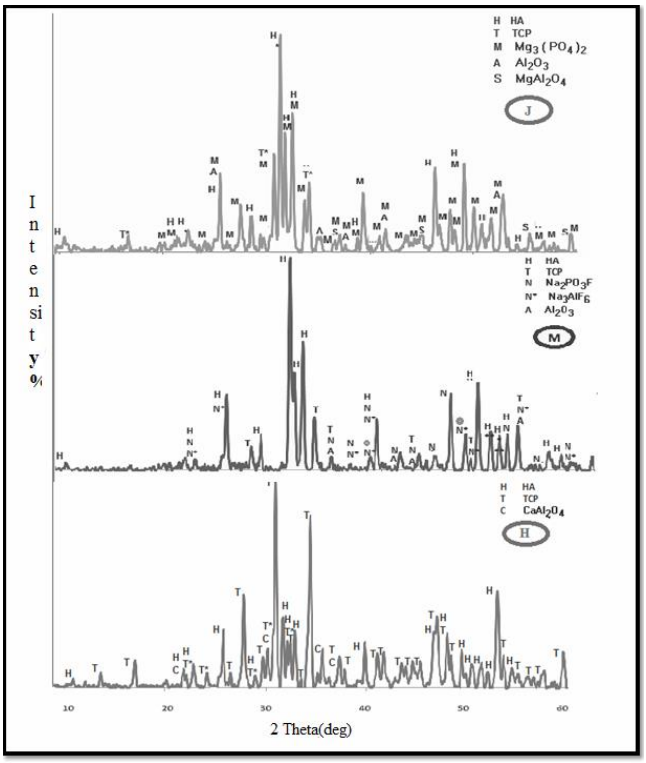

Fig. 1. X-ray diffraction pattern of the HA-Al_2O_3 nano composite powders with and without additives

Table 1. Comparing the crystalline sizes of H, J and M samples

Sample	Crystalline size (nm)	Crystalline Degree (%)
Sample H	54 nm	71
Sample J	41nm	76
Sample M	35 nm	84

which was due to the replacement of Cl^- to OH^- in HA crystal. By increasing $MgCl_2.6H_2O$, decomposition of HA decreased; therefore, the intensity peaks of HA phase increased. Also, by increasing NaF, the crystalline sizes decreased and the crystalline degrees of nanocomposites increased something which was due to the replacement of F^- to OH^- in HA crystal. By increasing NaF, decomposition of HA decreased and an intensity peak of HA phase was increased. Moreover, NaF as an additive had better effect on decreasing of crystalline size than $MgCl_2.6H_2O$, because the grain boundaries of NaF particles could prevented the growth of HA.

FTIR curves powder samples H, M and J were seen in Fig 2. The peak in the wave number of less than 500cm^{-1} was related to Al-O bond. The peak of P-O was related to phosphate groups at crystalline hydroxyapatite network in the wave numbers of 695 cm^{-1} and 831cm^{-1} the appeared peaks of J sample was related to the stretching vibration of Mg-O-Al bond. Peaks performed in 842cm^{-1} at FT-IR spectrum of H sample and peaks in the wave number of 831cm^{-1}, 964 cm^{-1} at FT-IR spectrum of sample J were belonged to the Al-O bond stretching vibration [30]. At the wave numbers of 964cm^{-1} and 960cm^{-1} the peaks related to Al_2O_3 phase were appeared with the addition of 10% $MgCl_2.6H_2O$ and NaF, respectively. Moreover, peak marked with P-H at the area of 2924cm^{-1} in the spectrum of sample of H and wave number of

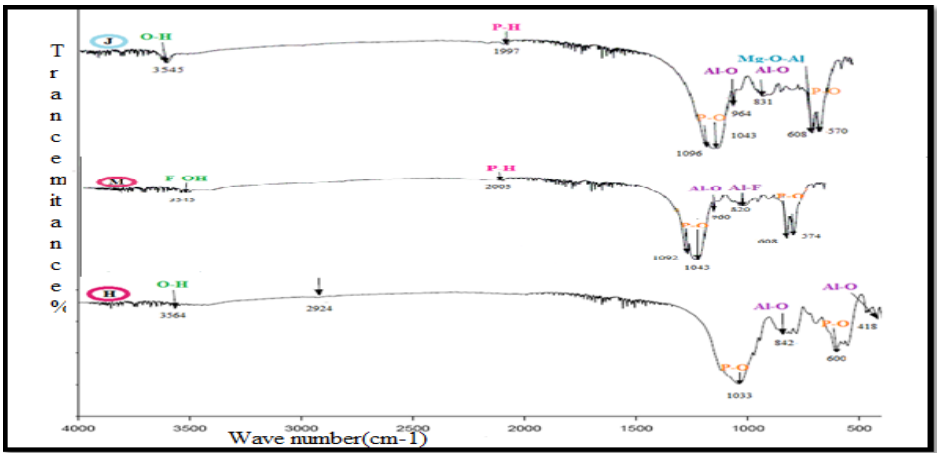

Fig. 2. FTIR curves of the HA- Al_2O_3 nano composite powders with and without additives

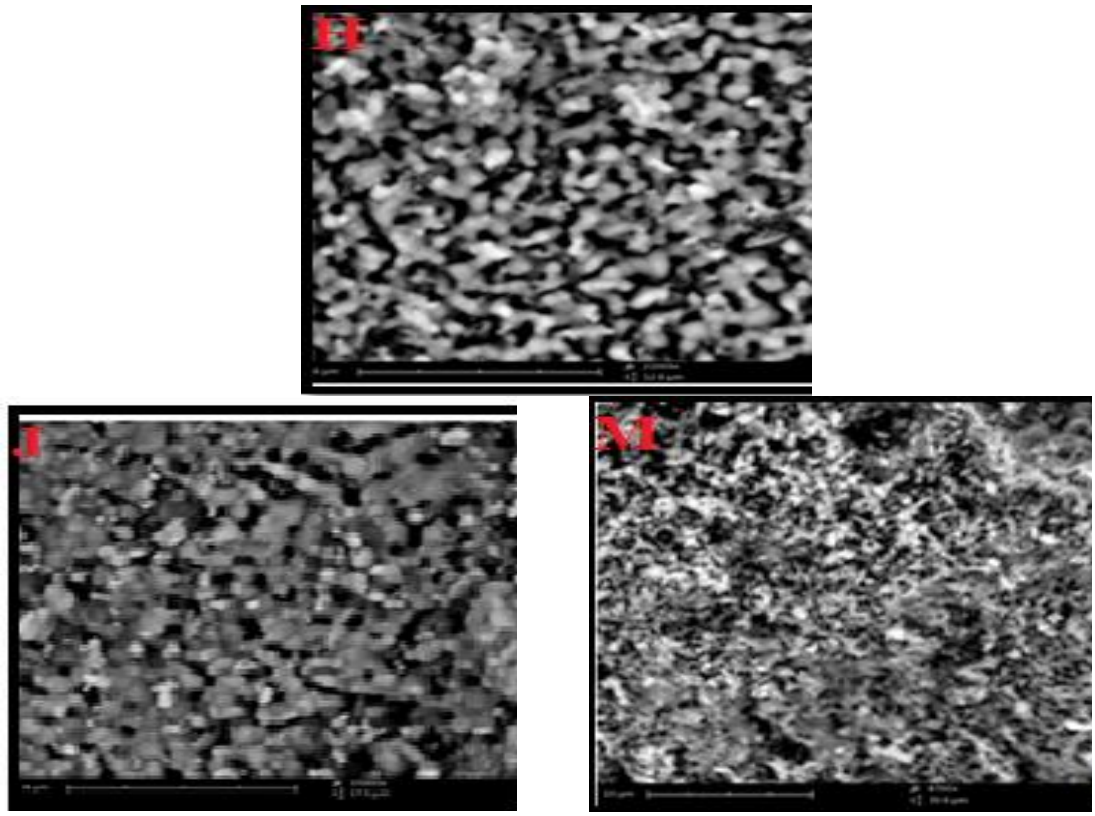

Fig. 3. FESEM images of sample H, J and sample M after calcination at 1200 °C temperature for 1 h

1997cm^{-1} at FT-IR spectrum samples of J and wave number of 2005cm^{-1} at FT-IR spectrum samples of M were related to HPO_4^{-2} groups [9].

Morphological properties of the HA-Al_2O_3 nano composite powder with different additives

Fig .3 shows the field emission scanning electron microscopy (FESEM) image of H, J and M samples with good dispersion and regular shape. Porous appearance with some agglomeration was seen in sample H. In sample J, in the presence additive of $MgCl_2.6H_2O$, particles with porous form indicated pirohydrolysis of magnesium chloride which resulted in the production of HCL gas

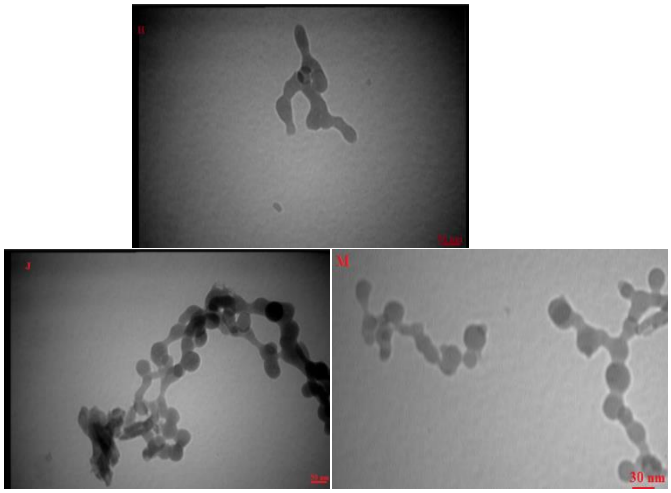

Fig. 4. TEM images of sample H, J and sample M after calcination at 1200 °C temperature for 1 h

that increased the pores and cracks in the surface of samples. However, in sample M had less porous appearance and with spherical shape.

Transmission electron microscopy (TEM) images of samples H (HA-Al_2O_3 nano composite powder), J (HA-Al_2O_3 nano composite powder with 10% of additive $MgCl_2.6H_2O$) and M (HA-Al_2O_3 nano composite powder with 10% of additive NaF) were used for investigating the particle size and morphology of nano composite powders in Fig 4.

As Fig 4 shows, the size of nanoparticles of sample H was about 50 nm with regular shape and some agglomeration. In sample J, in the presence additive of $MgCl_2.6H_2O$, particles formed with the sizes less than 45 nm and regular geometric shape; however, there was some agglomeration. In samples M, in the presence of surfactants and additive of NaF, the particle size was about 30 nm with regular geometric shape and without any agglomeration.

Morphological study of scaffold surface

The microstructures of the prepared scaffolds from the freewheeling casting method were studied by screens of field scanning electron microscopy (FESEM). As it was seen in FESEM images, the surface of all samples was completely porous. The existence of macroscopic cavities inside the scaffold created an interconnection between the porosity of the scaffolds. This interconnection was a vital parameter for cell infiltration, cell-to-scaffold attachment, nutrient transfer, and waste removal from metabolism and cell migration across a three-dimensional scaffold in the first days of placement of scaffold in the body. Another key parameter, in making the ideal scaffold was to apply porosity to texture engineering. The diameter of the porosity did not too large therefore, the cell could not attach to the wall of the scaffold for penetrating and growing. FESEM images in Fig 5 showed that, the size of porosity of SMA scaffolds (scaffold of chitosan / H A-Al_2O_3 with 10 % $MgCl_2.6H_2O$) was in the range of 100-150 μm which was the required porosity for bone application. Investigating the FESEM images of SFA scaffold (scaffold of chitosan / HA-Al_2O_3 with 10 % NaF) indicated the connection between the porosity of the scaffold and illustrated a significant increase in the internal connection of porosities (Fig 5.b).

Porosity measurement in this scaffold was indicated an increase in the diameter of the porosity of SFA scaffold compared to the SMA scaffold sample. The evaluation of SHA scaffold (scaffold of chitosan/ HA without additives) has shown that the various difference compared to other samples, especially in SFA scaffold. This difference was due to, the stronger binding of fluorine to the amine chitosan group relative to the hydroxide linkage with the amine group. In general, previous studies have shown that, the addition of nanoparticles into scaffolds led to a reduction in the porosity size which related to the study on chitosan gelatin scaffolds containing tricalcium phosphate nanoparticles and identified the addition of nanoparticles caused to reduce the porosity from about 128 to 157 μm to 104 to 137 μm [4, 26].

Porosity percentage of scaffolds

Another important parameter on the scaffold properties is the porosity of the scaffold, which has

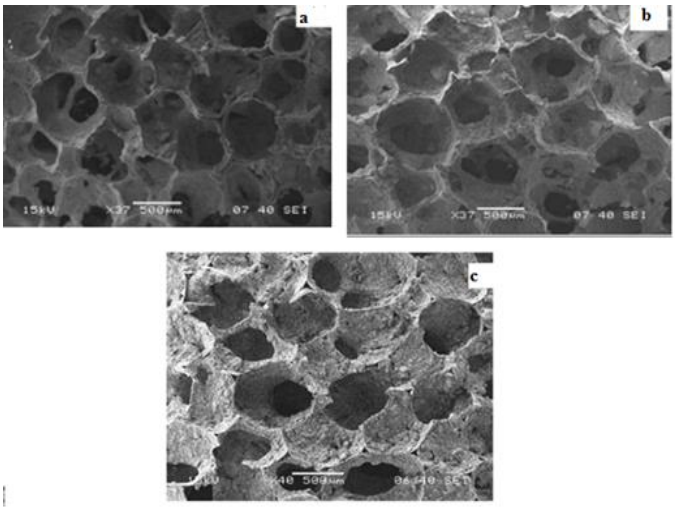

Fig. 5. FESEM images a) SMA b) SFA c) SHA scaffolds

a great impact on mechanical properties and being biocompatible. In order to calculate the porosity of scaffolds, the Archimedean method is used [31].

Studies have shown that, the porosity requirement for bone tissue for the correct reconstruction of normal bone tissue was about 45% to 65%. Low porosity prevented food from feeding, migrating, and disposing of appropriate cell materials. Also, the porosity percentage of extremely high scaffolding reduced the mechanical properties of the scaffold. Previous studies have shown that, the addition of ceramic particles could reduce the porosity and increase the strength of scaffold. Table 2 shows the porosities of the SHA, SFA, and SMA scaffolds. As it was shown, the porosity percentages of all scaffolds were within the porosity percentage required for bone scaffolds. However, the SMA scaffold with 70% porosity had the highest porosity percentage. Although this porosity could have the best effect on the survival rate of the cell and reduce the mechanical properties of the scaffold. Also, the SFA scaffold had 63% porosity, which was due to a stronger connection to the fluorine bond that confirmed the results of the presence and linkage of NAF and $MgCl_2$.

Table 2. The porosity percentages of different scaffolds

Sample	Porosity percentages (%)
SMA	± 3%70
SFA	± 4%63
SIIA	± 3%56

Mechanical properties of scaffolds

In addition to being biocompatible, the used scaffolds in tissue engineering should be mechanically matched to the tissue body. Bones are constantly under load and compressive forces; therefore, the compressive strength of scaffolds in bone tissue engineering is investigated. Although, the used material to make bone tissue engineering scaffolds and pore geometry had important role in primary cell adhesion, intracellular growth and blood capillaries. However, the porosity and porosity size influenced the mechanical properties of the scaffold. The optimal size and porosity were dependent on factors such as the nature of the materials and the conditions of the process for the construction of three-dimensional scaffolds. Previous studies have shown that, the use of ceramic particles increased the strength of polymer scaffolds. Chitosan was a polysaccharide polymer. This polymer had great potential for hydrogen bonding. The use of bio-polymers, especially chitosan, due to the hydrolysis of their bondage in the manufacture of scaffolds caused to reduce the mechanical properties of the scaffold. In Fig.6, the compressive strengths of the SMA, SFA, and SHA scaffolds are observed. The results indicated that, the compressive strength of the SMA scaffold had the least strength and the SFA scaffold had the highest compressive strength. This increase was due to the strong bonding of fluorine in SFA scaffold. Because fluoride was the most important element which could to supplement the bone [28].

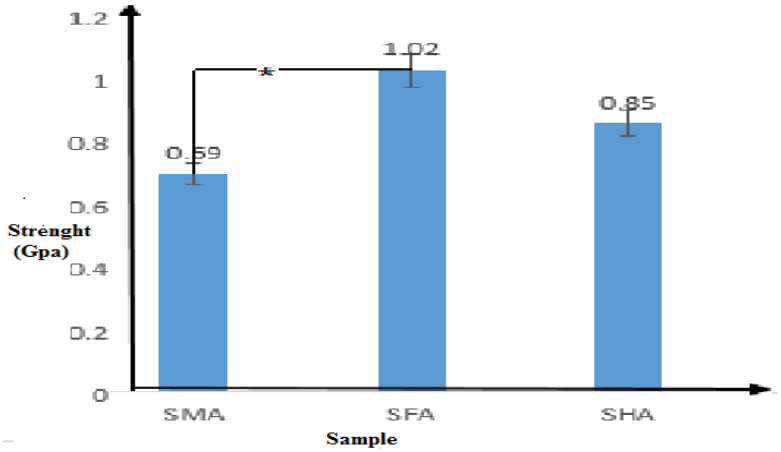

Fig. 6. Ultimate compressive strength diagram of scaffolds

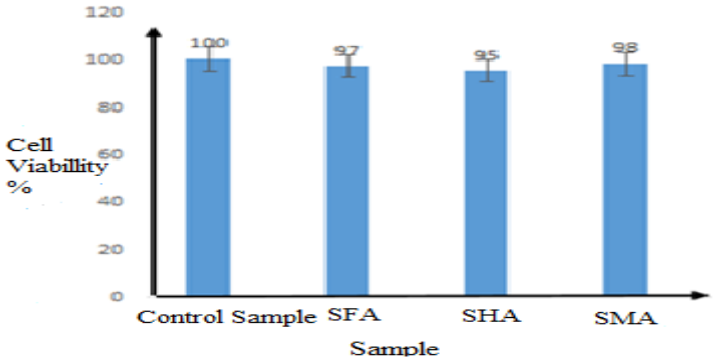

Fig. 7. Cell viability percentages of **control sample, SFA** , SHAand SMA scaffolds

Cell viability by tetrazolium assay

The survival and cell proliferation of SHA, SFA and SMA scaffolds were investigated by MTT after 3 days. As it was shown in Fig 7, the numbers of cells were increased in all samples after 3 days. Also, after three days of culture, there was no significant difference in survival between the cells. Previous studies have shown that, nano-sized apatite particles had the ability to bind to serum protein and growth factors that could activate cell differentiation. The results showed that, the cell viability for SMA scaffold was about 98% and SFA scaffold and SHA scaffold had the cell viability about 97% and 95% , respectively. This slight difference in the cellular residence rate was due to the formation of more porosity in SMA scaffold than other scaffolds.

Investigating and comparing the porosity of these three scaffolds with other scaffolds indicated that, the SMA scaffold had more porosity than other scaffolds that caused to be more appropriate than the other two scaffolds, and had the positive effect on the cellular residence rate. However, the increase in porosity also resulted in a significant reduction in the mechanical properties of the scaffold. In 2013-2018 researchers prepared different scaffolds an exhibited >80% porosity with a mean pore size range between 100 and 300 μm with maximum compressive strength of 2.2+_ 0.1 MPa, but, in our results , the compressive strength of scaffolds were in the rage of 0.59- 1.2 Gpa, that was more than pervious results. With comparing our results to previous results indicated, that our scaffold properties are near to previous scaffold properties which prepared by researchers.

CONCLUSION

Nano HA-Al_2O_3 nano composite powders with 10% additives of $MgCl_2.6H_2O$ and NaF were synthesized through precipitation method at 1200 °C. The particle size of nanocomposite containing 10% NaF as an additive was about 35 nm with

regular shape and good dispersion. In the next step, chitosan/ HA- Al_2O_3 scaffold was prepared by freeze casting method. The results showed that, the porosity of SMA scaffold was estimated to be in the range of 100-150 µm, which was close to the porosity particle size required for bone application. The porosity percentages of scaffold without additives was about 56% and with NaF as an additive was about 63 %, however, the scaffold with $MgCl_2.6H_2O$ additive with 70% porosity had the highest porosity percentage. The compressive strength of the SFA scaffold exhibited a two-fold strength compared to the SMA scaffold, which indicated the improved mechanical compatibility of the SFA scaffold. Cell culture results did not show any cell toxicity in both samples containing of $MgCl_2.6H_2O$ and NaF.

CONFLICT OF INTEREST

All authors declare that no conflicts of interest exist for the publication of this manuscript.

REFERENCES

1. Deng Z L , Sharff K A , Tang N I , Song W X , Luo J , Luo X , Xue A. Regulation of Osteopenia Differentiation During Skeletal Development. Front Biosci . 2008; 13(1) : 2001-2021.
2. Hesaraki S. Feasibility of alumina and alumina-silica nanoparticles to fabricate strengthened betatricalcium phosphate scaffold with improved biological responses. Ceramics International. 2016;42(6):7593-604.
3. Mitsionis AI, Vaimakis TC, Trapalis CC. The effect of citric acid on the sintering of calcium phosphate bioceramics. Ceramics International. 2010;36(2):623-34.
4. Kuttappan S, Mathew D, Nair MB. Biomimetic composite scaffolds containing bioceramics and collagen/gelatin for bone tissue engineering - A mini review. International Journal of Biological Macromolecules. 2016;93:1390-401.
5. Hirose S, Li M, Kojima T, de Freitas PHL, Ubaidus S, Oda K, et al. A histological assessment on the distribution of the osteocytic lacunar canalicular system using silver staining. Journal of Bone and Mineral Metabolism. 2007;25(6):374-82.
6. Pramanik S, Agarwal A K, Rai K N. Development of High Strength Hydroxyapatite for Hard Tissue Replacement . Trends in Biomaterilas. 2005 ; 19: 46-51.
7. - Sobczak-kuupiec A, Malina D, Kijkowska R .Comparative Study of Hydroxyapatite Prepared by the Authors with Selected Commercially Available Ceramics. Digest Journal of Nanomaterials and Biostructures. 2012 ; 7: 385-390.
8. Carano RAD, Filvaroff EH. Angiogenesis and bone repair. Drug Discovery Today. 2003;8(21):980-9.
9. Boden SD, Kang J, Sandhu H, Heller JG. Use of Recombinant Human Bone Morphogenetic Protein-2 to Achieve Posterolateral Lumbar Spine Fusion in Humans. Spine. 2002;27(23):2662-73.
10. Kim B-S, Sung H-M, You H-K, Lee J. Effects of fibrinogen concentration on fibrin glue and bone powder scaffolds in bone regeneration. Journal of Bioscience and Bioengineering. 2014;118(4):469-75.
11. Kim S-J, Bang H-G, Song J-H, Park S-Y. Effect of fluoride additive on the mechanical properties of hydroxyapatite/alumina composites. Ceramics International. 2009;35(4):1647-50.
12. Malorana C, Sigurtà D , Mirandola A , Garlini G , Santoro F. Sinus Elevation with Alloplasts or Xenogenic Materials and Implants: an up-to-4-year Clinical and Radiologic Follow-up. International Journal of Oral & Maxillofacial Implants. 2006; *21*(3):426-432.
13. Evis Z, Doremus RH. Effect of AlF3, CaF2 and MgF2 on hot-pressed hydroxyapatite–nanophase alpha-alumina composites. Materials Research Bulletin. 2008;43(10):2643-51.
14. Kim S-J, Bang H-G, Song J-H, Park S-Y. Effect of fluoride additive on the mechanical properties of hydroxyapatite/alumina composites. Ceramics International. 2009;35(4):1647-50.
15. Ghazanfari SMH, Zamanian A. Phase transformation, microstructural and mechanical properties of hydroxyapatite/alumina nanocomposite scaffolds produced by freeze casting. Ceramics International. 2013;39(8):9835-44.
16. Soh E, Kolos E, Ruys AJ. Foamed high porosity alumina for use as a bone tissue scaffold. Ceramics International. 2015;41(1):1031-47.
17. Ghosh D, Dhavale N, Banda M, Kang H. A comparison of microstructure and uniaxial compressive response of ice-templated alumina scaffolds fabricated from two different particle sizes. Ceramics International. 2016;42(14):16138-47.
18. Hu L, Zhang Y, Dong S, Zhang S, Li B. In situ growth of hydroxyapatite on lamellar alumina scaffolds with aligned pore channels. Ceramics International. 2013;39(6):6287-91.
19. Evis Z, Doremus RH. Effect of AlF3, CaF2 and MgF2 on hot-pressed hydroxyapatite–nanophase alpha-alumina composites. Materials Research Bulletin. 2008;43(10):2643-51.
20. Leilei Z, Hejun L, Kezhi L, Qiangang F, Yulei Z, Shoujie L. Synthesis and characterization of nanobelt-shaped Na, F and carbonate multi-substituted hydroxyapatite. Materials Letters. 2015;138:48-51.
21. Jia L, Duan Z, Fan D, Mi Y, Hui J, Chang L. Human-like collagen/nano-hydroxyapatite scaffolds for the culture of chondrocytes. Materials Science and Engineering: C. 2013;33(2):727-34.
22. Karri VVSR, Kuppusamy G, Talluri SV, Mannemala SS, Kollipara R, Wadhwani AD, et al. Curcumin loaded chitosan nanoparticles impregnated into collagen-alginate scaffolds for diabetic wound healing. International Journal of Biological Macromolecules. 2016;93:1519-29.
23. Maji K, Dasgupta S, Pramanik K, Bissoyi A. Preparation and Evaluation of Gelatin-Chitosan-Nanobioglass 3D Porous Scaffold for Bone Tissue Engineering. International Journal of Biomaterials. 2016;2016:1-14.
24. Deville S. Freeze-Casting of Porous Biomaterials: Structure, Properties and Opportunities. Materials. 2010;3(3):1913-27.
25. Kong L, Gao Y, Cao W, Gong Y, Zhao N, Zhang X. Preparation and characterization of nano-hydroxyapatite/chitosan composite scaffolds. Journal of Biomedical Materials Research Part A. 2005;75A(2):275-82.
26. Muthukumar T, Aravinthan A, Sharmila J, Kim NS, Kim J-H. Collagen/chitosan porous bone tissue engineering composite scaffold incorporated with Ginseng compound K. Carbohydrate Polymers. 2016;152:566-74.
27. Kim B-S, Kim JS, Chung YS, Sin Y-W, Ryu K-H, Lee J, et al.

Growth and osteogenic differentiation of alveolar human bone marrow-derived mesenchymal stem cells on chitosan/hydroxyapatite composite fabric. Journal of Biomedical Materials Research Part A. 2012;101A(6):1550-8.
28. Kutbay I, Yilmaz B, Evis Z, Usta M. Effect of calcium fluoride on mechanical behavior and sinterability of nano-hydroxyapatite and titania composites. Ceramics International. 2014;40(9):14817-26.
29. Du X, Wang Y, Su X, Li J. Influences of pH value on the microstructure and phase transformation of aluminum hydroxide. Powder Technology. 2009;192(1):40-6.
30. Tayebi S, Mirjalili F, Samadi H , Nemati A. The Effect of Additives on the Properties of HAp-Al_2O_3 Nano-Composite Powders. Journal of Ceramic Processing Research. 2016;17(10):1033-1041.
31. Wang T, Zhu X-K, Xue X-T, Wu D-Y. Hydrogel sheets of chitosan, honey and gelatin as burn wound dressings. Carbohydrate Polymers. 2012;88(1):75-83.
32. Hopkins GR, French SS, Brodie ED. Increased frequency and severity of developmental deformities in rough-skinned newt (Taricha granulosa) embryos exposed to road deicing salts (NaCl & MgCl2). Environmental Pollution. 2013;173:264-9.
33. Wang A-j, Paterson T, Owen R, Sherborne C, Dugan J, Li J-m, et al. Photocurable high internal phase emulsions (HIPEs) containing hydroxyapatite for additive manufacture of tissue engineering scaffolds with multi-scale porosity. Materials Science and Engineering: C. 2016;67:51-8.
34. Ghazanfari SMH, Zamanian A. Phase transformation, microstructural and mechanical properties of hydroxyapatite/alumina nanocomposite scaffolds produced by freeze casting. Ceramics International. 2013;39(8):9835-44.
35. Maroni A, Melocchi A, Parietti F, Foppoli A, Zema L, Gazzaniga A. 3D printed multi-compartment capsular devices for two-pulse oral drug delivery. Journal of Controlled Release. 2017;268:10-8.
36. Samal SK, Chiellini F, Bartoli C, Fernandes EG, Chiellini E. Hybrid Hydrogels Based on Poly(vinylalcohol)-Chitosan Blends and Relevant CNT Composites. Hydrogels: Springer Milan; 2009. p. 67-78.